

Private Eye: On the Limits of Textual Screen Peeking via Eyeglass Reflections in Video Conferencing

Yan Long*, Chen Yan†, Shivan Prasad*, Wenyuan Xu†, and Kevin Fu*

*Electrical Engineering and Computer Science, University of Michigan, Ann Arbor, USA

† College of Electrical Engineering, Zhejiang University, Hangzhou, China

{yanlong, shprasad, kevinfu}@umich.edu, {yanchen, wyxu}@zju.edu.cn

Abstract—Personal video conferencing has become the new norm after COVID-19 caused a seismic shift from in-person meetings and phone calls to video conferencing for daily communications and sensitive business. Video leaks participants’ on-screen information because eyeglasses and other reflective objects unwittingly expose partial screen contents. Using mathematical modeling and human subjects experiments, this research explores the extent to which emerging webcams might leak recognizable textual information gleaned from eyeglass reflections captured by webcams. The primary goal of our work is to measure, compute, and predict the factors, limits, and thresholds of recognizability as webcam technology evolves in the future. Our work explores and characterizes the viable threat models based on optical attacks using multi-frame super resolution techniques on sequences of video frames. Our experimental results and models show it is possible to reconstruct and recognize on-screen text with a height as small as 10 mm with a 720p webcam. We further apply this threat model to web textual content with varying attacker capabilities to find thresholds at which text becomes recognizable. Our user study with 20 participants suggests present-day 720p webcams are sufficient for adversaries to reconstruct textual content on big-font websites. Our models further show that the evolution towards 4K cameras will tip the threshold of text leakage to reconstruction of most header texts on popular websites. Our research proposes near-term mitigations, and justifies the importance of following the principle of least privilege for long-term defense against this attack. For privacy-sensitive scenarios, it’s further recommended to develop technologies that blur all objects by default, then only unblur what is absolutely necessary to facilitate natural looking conversations.

I. INTRODUCTION

Online video calls have become ubiquitous as a remote communication method, especially since the recent COVID-19 pandemic that caused almost universal work-from-home policies in major countries [25], [28], [35] and made video conference the new norm for companies and schools to accommodate interpersonal communications [7], [58]. This trend is predicted to continue even after the pandemic [5], [16].

While video conferencing provides people with the convenience and immersion of visual interactions, it unwittingly reveals sensitive textual information that could be exploited by a malicious party acting as a participant. Each video participant’s screen could contain private information. The participant’s own webcam could capture this information when it is reflected by the participant’s eyeglasses and unwittingly provide the information to the adversary (Figure 1). We refer

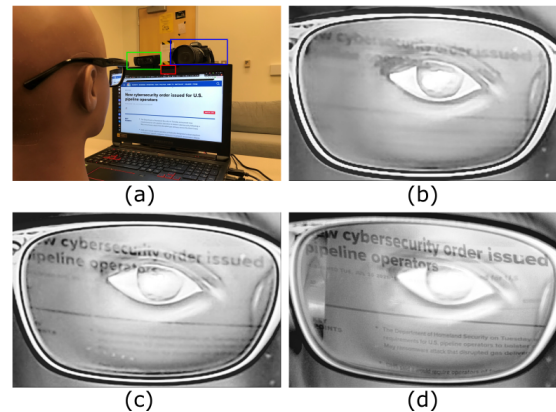


Fig. 1. The optical emanations of the victim’s screen are reflected by eyeglasses, captured by the victim’s webcam, and streamed to the adversary, which can then be used to reconstruct the screen contents. The experimental setup (a) with a laptop built-in webcam (b) (red box, 720p), an external Logitech webcam (c) (green box, 1080p), and a Nikon DSLR (d) (blue box, 4K) helps us predict the future fidelity of the attacks as video conferencing technologies evolve.

to this attack as a *webcam peeking attack*. Furthermore, it is important to understand the consequences and limits of webcam peeking attacks as adversary capability will only continue to increase with improvements to resolution, frame rate, and more.

Previous work shows that similar attacks exploiting optical reflection off nearby objects in controlled setups are feasible, such as observing teapots on a desk with high-end digital single-lens reflex (DSLR) cameras and telescopes at a distance [26], [27]. The challenge and characterization of webcam peeking, however, are qualitatively different due to the significantly lower quality images of present-day webcams compared to DSLRs. The lower-quality webcam images are caused by unique types of distortions, namely the shot and ISO noise due to insufficient light reception, and call for new image-enhancing techniques. In addition, new mathematical models and analysis frameworks are needed to understand the threat model of webcam peeking attack. Finally, this new threat model requires a dedicated evaluation to clarify the potential threats and mitigations to the average video conference user.

There are many types of media that can leak over optical reflections, including text and graphics. We focus on textual leakage in this work as it’s a natural starting point for measur-

able recognizability and modeling of the fundamental baseline of information leakage. We seek to answer the following three major questions: *Q1*: What are the primary factors affecting the capability of the webcam peeking adversary? *Q2*: What are the physical limits of the adversary’s capability in the present day and the predictable future, and how can adversaries possibly extend the limits? *Q3*: What are the corresponding threat of webcam peeking against cyberspace textual targets and the possible mitigations against the threat?

To answer *Q1*, we propose a simplified yet reasonably accurate mathematical model for reflection pixel size. The model includes factors such as camera resolution and glass-screen distance and enables the prediction of webcam peeking limits as camera and video technology evolve. By using the complex-wavelet structural similarity index as an objective metric for reflection recognizability, we also provide semi-quantitative analysis for other physical factors including environmental light intensity that affect signal-to-noise ratio of the reflection light. To answer *Q2*, we analyze the distortions in the webcam images and propose multi-frame super resolution reconstruction for effective image enhancing to extend the limits. We then gather eyeglass reflection data in lab environments and evaluate the recognizability limits of the reflections through both crowdsourcing workers on Amazon Mechanical Turk and optical character recognition models. The evaluation shows it is possible with over 75% accuracy to recognize texts that have a physical height of 10 mm with a 720p webcam. To answer *Q3*, we focus on web textual targets to build a benchmark that enables meaningful comparisons between present-day and future webcam peeking threats. We first map the limits derived from the model and evaluations to web textual contents by surveying previous reports on web text size and manually inspecting fonts in 117 big-font websites. Then, we conduct a user study with 20 participants and play a challenge-response game where one author acts as an adversary to infer HTML contents created by other authors. Results of the user study suggest that present-day 720p webcams can peek texts in the 117 big-font websites and future 4K webcams are predicted to pose threats to header texts from popular websites. We also investigate the underlying factors enabling easier webcam peeking in the user study by analyzing the correlation between adversary recognition accuracy and multiple factors. We found, for example, user-specific parameters including browser zoom ratio plays a more important role than the glass-screen distance. Finally, we investigate possible near-term mitigations including adjusting environmental lighting and blurring the glass area in software. We also envision long-term solutions following a principle of least privilege. In summary, the goal of this work is to provide theoretical foundation and benchmark for the study on emerging webcam peeking threats with evolving webcam technologies and the development of securer video conferencing infrastructures. We summarize our main contributions as follows:

- Our work quantifies the limits and primary factors that predict the degree of information leakage from webcam

peeking by using theoretical modeling and experimentation. This characterization helps predict future unknown vulnerabilities tied to the limits of evolving webcam technologies that do not yet exist.

- A benchmark centering on web textual targets that enables comparisons of webcam peeking threats. Our benchmarking methodology builds upon web text design conventions and a 20-participant user study on present-day cameras such that the benchmark can be applied to both hypothetical and emerging cameras in the coming years.
- Analysis on near-term mitigations including using software-based blurring filters and changing physical setups as well as possible long-term defenses by following a principle of least privilege. Our analysis investigates the potential effectiveness and implementation methods of different protection approaches.

II. THREAT MODEL & BACKGROUND

A. Threat Model

In this work, we study the webcam peeking attack during online video conference, where the adversary and the victim are both participants. We assume the device the victim uses to join the video conference consists of a display screen and either a built-in or an external webcam that is mounted on the top of the screen as in most cases, and the victims wear glasses with a reflectance larger than 0, i.e., at least a portion of the light emanated by the monitor screen can be reflected from the glasses to the webcams. We do not enforce constraints on the devices used by the adversary. When the adversary launches the attack, we assume the victim is facing the screen and webcam in the way that the screen emanated light has a single-reflection optical path into the webcam through glasses lens outer surface. We do not assume the adversary has any control or information on the victim’s device.

We assume that the victim’s up-link video stream is enabled during the attack, and the adversary can acquire the down-link video stream of the victim. The adversary can achieve that by either directly intercepting the down-link video stream data, or recording the victim’s video with the video conferencing platform being used or even third-party screen recording services. Since the webcam peeking attack does not require active interaction between the victim and the adversary, the adversary does not need to attempt a real-time attack, but can store the video recording and analyze the video frames off-line.

B. Glasses

Glasses modify the light passing through and reflected by the lenses in different ways depending on the purpose of the glasses. The most common types of glasses that people wear in an video conferencing setting are prescription glasses and blue-light blocking (BLB) glasses. Research shows that over 25% of world population wear prescription glasses and the percentage is estimated to grow to over 50% by 2050 [47]. BLB glasses, which are made of lenses able to reflect visible blue light (with a wavelength of about 400-500 nm), has also been estimated

to have a global market of 22 million by 2025 [12], [57] due to the preliminary verification of its potential to prevent photo-chemical damages to retina [42]–[44]. BLB glasses come in two forms, namely standalone non-prescription (flat) glasses and BLB coating that can be added to traditional prescription glasses. The reflectance and curvature of glass lenses are the two most important characteristics in the process of reflecting screen optical emanations.

Reflectance. Reflectance of a lens surface is the ratio between the light energy reflected and the total energy incident on a surface [6]. Reflectance is wavelength-dependent, which can be viewed as a transfer function on the light spectrum. Theoretically, the higher the reflectance, the more light can be reflected and captured by a webcam. Prescription glasses normally have a reflectance higher than 10% in the visible light spectrum with the highest reflectance being in the green and blue-light range [6], [56]. Previous researches show that commercial BLB glasses often have about 50% reflectance in the blue-light spectrum [31], [52].

Curvature. Curvature of a lens surface is the reciprocal of the approximated radius of the surface, representing how much it deviates from a plane. Since the most reflective part of the glasses is often the outer surfaces of the lenses which are mostly convex, a lens can be approximated as a convex mirror with a focus length of half of the radius. Smaller curvature (larger radius and focal length) leads to larger-size reflections. Researches show that the curvature of different types of glasses vary but generally have a radius larger than 20 cm [33], [68].

C. Digital Camera Imaging System

A digital camera is an optical system that converts light to digital signals and storage. A digital camera is often composed of a lens for focusing and controlling the amount of light passed into the imaging system, and subsequent imaging sensors that pick up the light and generate electric signals. The electric signals will then go through signal conditioning paths and analog-to-digital converter of the camera, and be stored or processed as digits. Digital cameras usually have millions of sensing units uniformly distributed on the sensor plane, each of which is a Charge-coupled Device (CCD) or Complementary Metal-oxide-semiconductor (CMOS) unit that converts the energy of the photons it receives within a certain period of time, i.e., the exposure time, to an amplitude-modulated analog signal. Each sensing unit then corresponds to a “pixel” in the digital domain. Theoretically, the more sensing units a camera sensor has, the higher pixel resolution its digital images are. Mainstream 720p, 1080p, 4K cameras typically have 1280×720, 1920×1080, and 3840×2160 such sensing units respectively. The quality of a digital image to human perception is mainly determined by its pixel resolution, color representation, the amount of received light that are of our interests, and various imaging noise. While pixel resolution and color representation are often already decided by the imaging hardware, the users can control 3 key parameters to adjust the light reception and related imaging noise, namely

aperture size, exposure time, and ISO value. The last two parameters are closely related to webcam peeking attack.

Exposure Time. Theoretically, the longer the exposure time, the more photons will hit the imaging sensors and thus there can be potentially more light of interest captured. The images with a longer exposure time will generally be brighter. The downside of having a longer exposure time is the aggravated motion blur when imaging a non-still object.

ISO Value. The ISO value represents the amplification factor of the photon-induced electrical signals. In darker conditions, the user can often make the images brighter by increasing the ISO value. However, the downside of having higher ISO is the simultaneous amplification of various imaging noise.

D. Text Size Representations

The size of the smallest recognizable texts is a key metric for the limits of the webcam peeking attack explored in this work. It is thus important to select proper representations of text size. Texts in this work exist in both digital and physical domain and it is necessary to find representations in both domains to understand the mechanism of webcam peeking. When texts are digital, i.e., in the victim’s software such as browsers and in the webcam image acquired by the adversary, we use point size and pixel size to represent the text size respectively. Using point size on the user side is because it is the software representation/unit that users are most familiar with and thus help users to better understand the threat of this attack. Using pixel size on the adversary side is because it is intuitive for the adversaries to interpret the reflected targets as pixels in the images, especially when the reflections are as small as having a height of several pixels. Finally, in the physical domain, i.e., when the texts are displayed on users’ screens as physical objects, we use the cap height of the fonts and the physical unit mm to represent the size as it is invariant across different computer displays and enable quantitative analysis of the threats. Cap height is the height of capitalized letters. In a certain font (when font style and size are specified), all uppercase letters are of the same height. As a result, cap height is usually used as a convenient representation of physical text size and the base for other font parameters such as spacing and stroke width [23], [24]. The non-trivial conversion between these three representations will be detailed in Section III-B.

III. WEBCAM PEEKING THROUGH GLASSES

In this section, we start with a feasibility test that reveals the 3 key building blocks of the webcam peeking threat model, namely (1) reflection pixel size, (2) viewing angle, and (3) light signal-to-noise ratio (SNR). For the first two building blocks, we develop a mathematical model that quantifies the related impact factors. For light SNR, we analyze one major factor it encompasses, i.e., image distortions caused by shot noise, and investigate using multi-frame super resolution (MFSR) to enhance the reflection images. We will analyze other physical factors affecting light SNR in Section IV-E. By default, all experiments until Section IV are conducted with the Acer

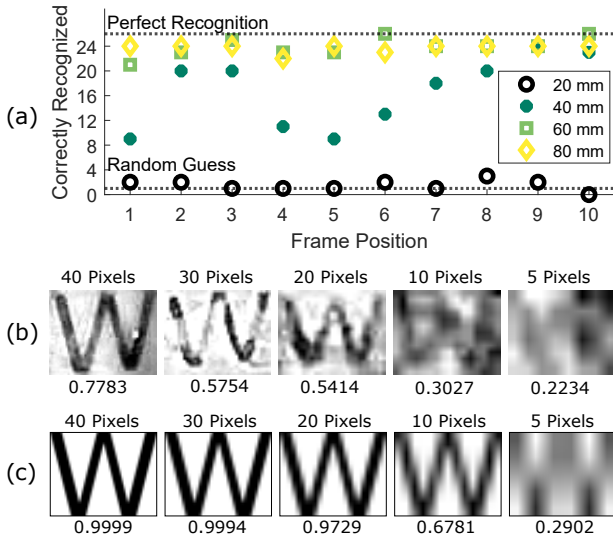


Fig. 2. (a) The number of correctly recognized letters out of 26 with different sizes (heights) in the feasibility test. Recognizing even 20 mm texts are found difficult without image enhancing. 10 mm’s result is trivial and thus omitted. (b) The captured images of the reflections. Comparing with the ideal reflections, additional distortions exist that undermine the image recognizability. (c) The estimated ideal reflections in the feasibility test corresponding to letters with a height of 80, 60, 40, 20, 10 mm respectively. The images are subjected to aliasing when enlarged.

laptop with its built-in 720p webcam, the pair of BLB glasses, and the pair of prescription glasses described in Appendix B.

A. Feasibility Test

We conduct a feasibility test of recognizing single alphabet letters with a template matching algorithm that performs non-rigid registration, calculates 2D cross-correlation between the reflections and templates, and classifies the reflections. With a similar setup as in Figure 1, a mannequin wears the BLB glasses with a glass-screen distance of 30 cm. We display the 26 capital letters one at a time on the laptop screen with cap heights of 80, 60, 40, 20, and 10 mm, and capture each display’s reflections from 10 different frame positions by manually moving the mannequin slightly between each two frames to emulate the effect of minor head movements of a human. Figure 2 (a) shows the recognition results, which suggests that recognizing texts as large as 20 mm is difficult for the template matching program.

To analyze the reasons for such difficulty and identify the key building blocks, we inspect the captured texts as shown in Figure 2 (b). We find that the 5 different cap heights resulted in letters with heights of 40, 30, 20, 10, and 5 pixels in the captured images. As expected, texts represented by fewer number of pixels are harder to recognize both for the template matching algorithm and human. The reflection pixel size acquired by adversaries is thus one key building block of the characteristics of webcam peeking attack that we need to model. Modeling how reflection pixel size changes with textual targets, webcams, glasses, and distances will also allow us to generalize results acquired in a certain setup to other conditions without repeating the experiments. In addition, Figure 2 (c) shows the ideal reflections with these pixel sizes

TABLE I
PARAMETERS FOR MODELING REFLECTION PIXEL SIZE

Notation	Parameter
h_o	Physical size (cap height) of the object on the screen
h_s	Physical size of the object’s projection on the sensor
s_p	Pixel size of the imaged object
h_i	Physical size of the object’s virtual image
P	Physical size of a single imaging sensor pixel
N	Number of pixels the camera has in the dimension
W	Physical size of the imaging sensor in the dimension
f	Camera focal length
d_o	Distance between screen and glasses
d_i	Distance between glasses and virtual image
f_g	Focal length of the glasses convex outer surface

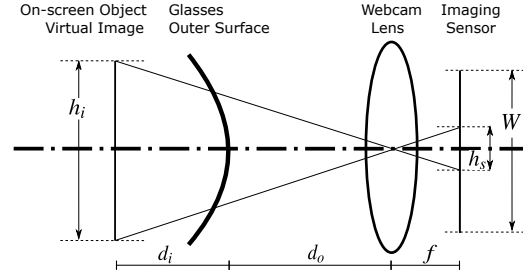


Fig. 3. The model of reflection pixel size. To better depict the objects, the sizes are not drawn up to scale. The screen overlaps with the webcam lens and is omitted in the figure.

by resampling the template image. Comparing (a) and (b), we notice small-size texts are subjected to additional distortions besides the issue of small pixel resolution and noise caused by the face background, resulting in bad signal-to-noise ratio (SNR) of the textual signals. To quantify the difference, we use the complex-wavelet structural similarity (CWSSIM) score between the template and resampled/captured images as an objective metric of the reflection quality (Appendix G), and show the scores under each image. The differences show that the SNR of reflected light corresponding to the textual targets is another key building block we need to characterize. Finally, we notice that when we rotate the mannequin with an angle exceeding a certain threshold, the webcam images do not contain the displayed letters on the screen anymore. It suggests that the viewing angle is another critical building block of the webcam peeking threat model which acts as an on/off function for successful recognition of screen contents. In the follow sections, we seek to characterize these three building blocks.

B. Reflection Pixel Size

In the attack, the embodiment of textual targets undergoes a 2-stage conversion process: digital (victim software) → physical (victim screen) → digital (adversary camera). In the first stage, texts specified usually in point size in software by the user or web designers are rendered on the victim screen with corresponding physical cap heights. In the second stage, the on-screen texts get reflected by the glass, captured by the camera, digitized, and transferred to the adversary’s software as an image with certain pixel sizes. Generally, more usable pixels representing the texts enable adversaries to recognize

texts more easily. The key is thus to understand the mechanism of point size \rightarrow cap height \rightarrow pixel size conversion.

Point Size \rightarrow Cap Height. Mapping between digital point size and physical cap height is not unique but dependent on user-specific factors and software. The conversion formula for most web browsers can be summarized as follows:

$$h_o = \frac{4}{3} p_t \cdot \frac{H_{scr}}{N_{os}} \cdot s_{os} \cdot s_b \cdot r_{cap} \quad (1)$$

where h_o is the physical cap height of the text, $\frac{4}{3} p_t$ is the number of display hardware pixels most web browsers use to render the text given a point size p_t , H_{scr} is the physical height of the screen, N_{os} is the screen resolution on the height dimension set in the OS which can be equal to or smaller than the maximum supported resolution, s_{os} and s_b are the OS and browser zoom/scaling ratios respectively, and r_{cap} is the ratio between the cap height and the physical point size which is on average $\frac{2}{3}$ [23], [24].

Cap Height \rightarrow Pixel Size. We would like to remind the readers that we only use pixel size to represent the size of texts living in the images acquired by the adversary¹. Figure 3 shows the model for this conversion process. To simplify the model, we assume the glasses lens, screen contents, and the webcam are aligned on the same line with the same angle. The result of this approximation is the loss of projective transformation information, which only causes small inaccuracies for reflection pixel size estimation in most webcam peaking scenarios. Figure 3 only depicts one dimension out of the horizontal and vertical dimensions of the optical system, but can be used for both of the dimensions. In this work we focus on the vertical dimension for analysis, i.e., the reflection pixel size we discuss is the height of the captured reflections in pixels. We summarize the parameters of this optical imaging system model in Table I. By trigonometry, we know

$$\begin{cases} \frac{h_s}{f} = \frac{h_i}{d_o + d_i} \\ h_s = s_p P \\ P = \frac{W}{N} \end{cases} \Rightarrow s_p = \frac{h_i}{d_o + d_i} \cdot \frac{f}{W} \cdot N \quad (2)$$

As pointed out in Section II-B, the reflective outer surface of glasses are mostly convex mirrors which shrink the size of the imaginary object h_i and also decreases d_i compared to an ideal flat mirror. To calculate the reflection pixel size s_p in this case, we can use the convex mirror equations [45]

$$\begin{cases} \frac{1}{(-f_g)} = \frac{1}{d_o} + \frac{1}{(-d_i)} \\ \frac{h_i}{h_o} = \frac{d_i}{d_o} \end{cases}$$

¹Since web/software designers sometimes also directly specify text size in pixel size ($\frac{4}{3} P_t$ in Equation 1), the two pixel sizes can be easily confused without explanation.

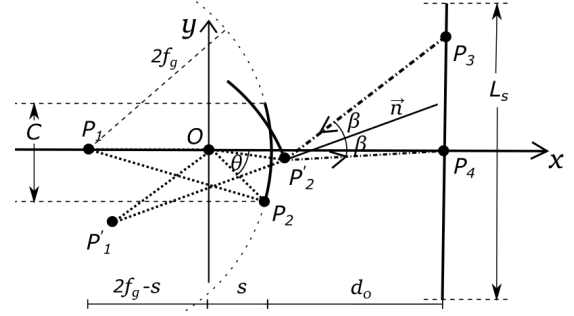


Fig. 4. The model of viewing angle.

TABLE II
THE PREDICTED FEASIBLE ATTACK RANGES FOR THE VIEWING ANGLE.

Type	Theoretical	Measurement
Pres: All Page + Horizontal	$\pm 15^\circ$	$\pm 17^\circ$
Pres: Center + Horizontal	$\pm 5^\circ$	$\pm 8^\circ$
Pres: All Page + Vertical	$\pm 9^\circ$	$\pm 13^\circ$
Pres: Center + Vertical	$\pm 3^\circ$	$\pm 5^\circ$
BLB: All Page + Horizontal	$\pm 20^\circ$	$\pm 25^\circ$
BLB: Center + Horizontal	$\pm 10^\circ$	$\pm 13^\circ$
BLB: All Page + Vertical	$\pm 14^\circ$	$\pm 19^\circ$
BLB: Center + Vertical	$\pm 8^\circ$	$\pm 10^\circ$

where f_g is the focal length of the convex mirror which is half of the radius of the glasses lens and is defined to be positive. Plugging the above equations into Equation 2 we can then get

$$s_p = \frac{h_o f_g}{d_o^2 + 2d_o f_g} \cdot \frac{f}{W} \cdot N, \quad (3)$$

The term $\frac{f}{W}$ of typical laptop webcams can be estimated to be in the range 1.1 – 1.4 (see Appendix C). With the Acer laptop and BLB glasses and a glass-screen distance of $d_o = 30$ cm, the estimated vertical pixel size of a 20 mm-tall object displayed on screen is in the range of 9.2 – 11.7 pixels, which matches with the 10 pixels found in the feasibility test and verifies the accuracy of the model despite the approximation we made.

C. Viewing Angle

To model the effect of viewing angle, we construct a 2D coordinate system as shown in Figure 4. Similar to the pixel size model, we only use 2D modeling for simplicity which can represent either horizontal or vertical rotations, and we only consider one glass lens since the two lenses are symmetric. The lenses are further modeled as spherical with a radius $2f_g$. We set the origin O to the center of the head which is also treated as the rotation center, and assume the initial orientation without rotation is such that the center of the glass lens arc P_1 aligns with the rotation center and the laptop webcam P_4 on the X-axis. The distance between the glass lens center and the rotation center is s . To calculate the maximum feasible angles, we only need to consider the reflections from either one of the two boundary points of the glass lens since they are symmetric. We label the bottom boundary point as P_2 . After a rotation of angle θ , P_1, P_2 are rotated to P_1', P_2' respectively, and the vector $\overrightarrow{P_1' P_2'}$ yields the normal \vec{n} at the reflection point P_2' . P_3, P_4 denote the point source on the screen whose light gets

reflected to the camera with an incident angle β . With L_s being the length of the screen on the dimension, the camera should be able to peek reflections from the glass lens if P_3 falls in the range of the screen. C denotes the length of the chord formed by the glass lens. A detailed derivation of the viewing angle model can be found in Appendix D.

To estimate the range of angle that enables webcam peeking attack, we consider two cases of successful peeking with a rotation. The first case All Page claims success as long as there exists a point on the screen whose emitted light ray can reach camera (P_4). The second case Center claims success only if the contents at the center of the screen (when P_3 overlaps with P_4) has emitted lights that can be reflected to camera. Table II summarizes the calculated theoretical angle ranges and the measured values. We note that the measured ranges are uniformly larger than the theoretical values, which could be caused by a coarse estimate of the distance s since the actual distance between the lens and the rotation center is hard to determine, and the fact that the model approximates the camera as a point instead of a surface. Nevertheless, both the theoretical model and measurements show that the webcam peeking attack is relatively robust to human positioning with different head viewing angles, which is validated later by the user study results (Section V-B).

D. Image Distortion Characterization

Compared to reflection pixel size and viewing angle, factors affecting the light SNR of reflections is harder to fully quantify as it requires accurate optical models for the imaging sensors which are device-dependent. We thus aim to offer semi-quantitative analysis and start by focusing on the image distortion factor, since understanding the source of image distortions provides us with insights into the ways an adversary may improve the reflection quality and thus extend the limits of webcam peeking. We will study the other environmental factors in Section IV-E.

Generally speaking, the possible distortions are composed of external distortions and the imaging systems' inherent distortions. External distortions mainly include factors like motion blur caused by normal small-amplitude tremor of human body [37] and intentional large-amplitude body movements that occasionally occur. The latter is not a focus of this work due to its random and occasional characteristic. On the other hand, imaging systems' inherent distortions mainly include out-of-focus blur and various imaging system noise.

To determine the dominant types of distortions, we recorded videos with the laptop webcam and a Nikon Z7 DSLR [17] representing a higher-quality imaging system. The setup is the same as above except we tested with both the still mannequin and a human to analyze the effects of human tremor. We also taped the inner surface of the glasses lens with black papers in order to eliminate the impact of the face background and better characterize the inherent distortions. Effects of the face background will be discussed in Section IV-E. The webcam and Nikon Z7 were set to the same color temperature (3500 K) and frame rate (30 fps). For the highly configurable Nikon Z7,

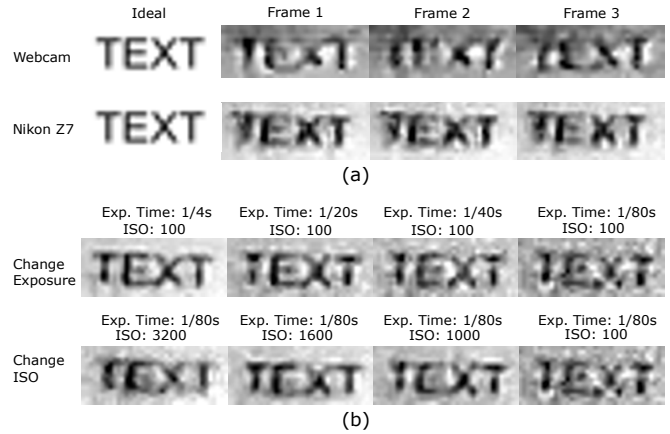


Fig. 5. (a) The ideal capture versus the actual captures in three consecutive frames by webcam (1st row) and Nikon Z7 (2nd row). The distortions feature occlusions with inter-frame and intra-frame variance. The webcam yields larger variance. (b) Photos captured by Nikon Z7 under different exposure time and ISO settings. Longer exposure time and medium ISO yield smaller distortions and increase SNR.

we set the ISO, aperture, and exposure time to 100, $F4$, and $\frac{1}{30}s$ respectively, disabled all active noise-reduction schemes including vibration reduction, and used manual focus mode. For both cases, we displayed the string “TEXT” and adjusted the size to make sure the captured text in both cameras’ frames have a size of 10 pixels vertically. Figure 5 (a) shows the comparison between the ideal reflection capture and the actual captures in three consecutive video frames of the webcam (1st row) and Nikon Z7 (2nd row) with the human. We observed the following three key features of the video frames in this setup with both the mannequin and human:

- Motion and out-of-focus blurs are generally negligible.
- Inter-frame variance: The distortions at the same position of each frame are different, generating different noise patterns for each frame.
- Intra-frame variance: Even in a single frame, the distortion patterns are spatially non-uniform.

Different from previous works [26], [27], motion blur and out-of-focus blurs that are theoretically uniform within a single frame are not the limiting factors in the webcam peeking threat model because of the short exposure time and relatively close and constant camera-object distance. Instead, distortions with intra-frame and inter-frame variance dominate which suggests the image quality cannot be easily improved with PSF deconvolution as in [26] and new image enhancing techniques are needed. One key observation is that the captured texts are subjected to occlusions (the missing or faded parts) caused by shot noise [19] when there is insufficient number of photons hitting the sensors. This can be easily reasoned in light of the short exposure time and small text pixel size causing reduced photons emitted and received. In addition, other common imaging noise such as Gaussian noise gets visually amplified by relatively higher ISO values due to the bad light sensitivity of the webcam sensors. We call such noise as ISO noise. Both the two types of distortions have the potential to cause intra-frame and inter-frame variance. Figure 5 (b) taken with the configurable Nikon Z7 shows how these two forms of

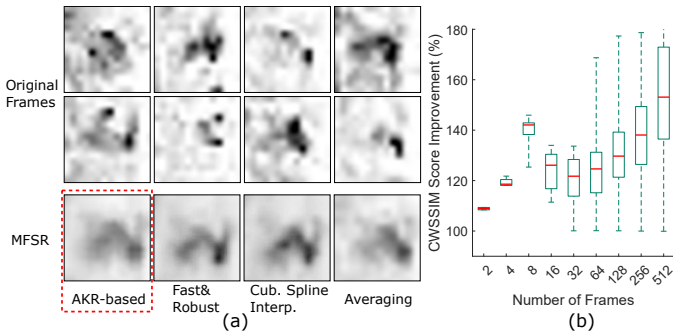


Fig. 6. (a) Comparison between single frames and the MFSR-reconstructed images with 4 different MFSR approaches. The MFSR images are reconstructed with the 8 frames shown at the top. The AKR-based approach generally produces the best reconstruction results in our task of reflection image reconstruction. (b) The improvement of reflection reconstruction quality as the number of frames used for MFSR increases.

distortions affect the images. For the first set of images (1st row), we keep ISO at 100 and decrease the exposure time from $\frac{1}{4}s$ to $\frac{1}{80}s$ to show the effect of fewer photons hitting the image sensors which results in increased shot noise occlusions. For the second set of images (2nd row), we keep the exposure time at $\frac{1}{80}s$ while increasing ISO from 100 to 3200 to show the effect of increased ISO noise. The shot and ISO noise in the webcam peeking attack plays on a see-saw with an equilibrium point posed by the quality of the camera imaging sensors. It suggests that the threat level will further increase (see comparison between the webcam and Nikon Z7’s images in Figure 5) as future webcams are equipped with better-quality sensors at lower costs.

E. Image Enhancing with MFSR.

The analysis of distortions calls for an image reconstruction scheme that can reduce multiple types of distortions and tolerate inter-frame and intra-frame variance. Such a multi-fold reconstruction problem is highly challenging from the standpoint of reverting the physical distortion processes in the digital domain. Inspecting the reflection reconstruction problem from a general information theory perspective, we know the prior knowledge of the physical processes offer additional entropy. Without such prior, we need to utilize entropy existing in the captured video frames. This brings us back to the observation from Figure 2 (a), that different frame positions yield different recognition accuracy which suggests each frame may possess unique information. It’s thus intuitive to reconstruct a better-quality image from multiple low-quality frames. Such reconstruction problem is usually defined as multi-frame super resolution (MFSR) [67]. The basic idea is to combine non-redundant information in multiple frames to generate a better-quality frame. The formulation of the MFSR problems often take into consideration various distortions to the images such as blur effects and other general noise. The reconstruction problem can be formulated as

$$\hat{I}_H = \min_I \sum_{k=1}^M \left\| P_k(I) - I_L^k \right\| \quad (4)$$

where \hat{I}_H is the estimated high-resolution image, I_L^k is the k -th low-resolution image, and $P_k(\cdot)$ encodes various distortion terms.

We tested 3 common light-weight MFSR approaches that do not require a training phase, including cubic spline interpolation [67], fast and robust MFSR [40], and adaptive kernel regression (AKR) based MFSR [48]. Tests results on the reflection images show that the AKR-based approach generally yields better results than the other two approaches in our specific application and setup. All the three approaches outperform a simple averaging plus upsampling of the frames after frame registration, which may be viewed as a degraded form of MFSR. An example of the comparison between the different methods and the original 8 frames used for MFSR are shown in Figure 6 (a). We thus use the AKR-based approach for the following discussions.

One of the most important parameter to decide for the use of webcam peeking is the number of frames used to reconstruct the high-quality image. Figure 6 (b) shows the CWSSIM score improvement of the reconstructed image over the original frames with different number of frames used for MFSR when a human wears the glasses to generate the reflections. Note that increasing the number of frames do not monotonically increase the image quality since live victims’ movements can degrade the image registration step in the MFSR process and thus undermine the reconstruction quality. Based on the results, we empirically choose to use 8 frames for the following evaluations. In addition, the improvement in CWSSIM scores also validates that MFSR-resulted images have better quality than most of the original frames. We thus only consider evaluation using the MFSR images in the following sections.

IV. REFLECTION RECOGNIZABILITY IN CONTROLLED SETUPS

In this section, we evaluate the recognizability of reflected texts enhanced by the MFSR method given a specific set of webcam, glasses, and environmental conditions. We then investigate the impact of the most significant factors. The evaluations in this section are performed in a controlled lab environment and serve as the foundation for the analysis in Section V.

A. Experimental Setup

Equipment. We collected all data with the aforementioned Acer laptop as the victim device, and another Samsung laptop [18] as the adversary’s device. The two laptops were in a lab environment with WiFi network connection. The victim laptop was measured to have an internet download speed of 246 Mbps and upload speed of 137 Mbps while those for the adversary laptop were 144 Mbps and 133 Mbps respectively. We used two pairs of glasses, i.e., the pair of BLB glasses and prescription glasses.

Data Collection. We asked a person to wear the glasses and sit in front of the victim laptop. The glass-screen distance was chosen to be 40 cm which was also found to be close to the average distance in the user study (see Figure 11 (b)).

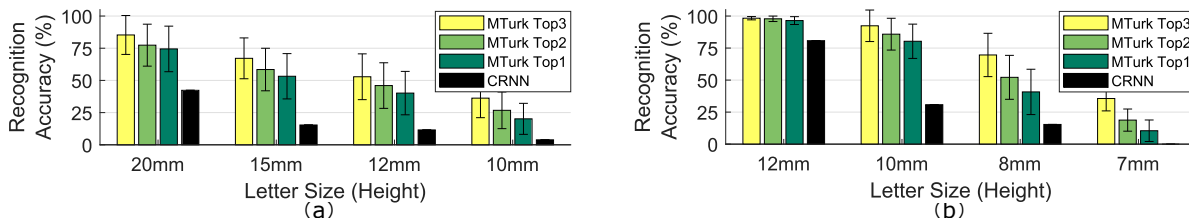


Fig. 7. The recognition accuracy of letters in different sizes with (a) the BLB glasses and (b) the prescription glasses. Although the pair of BLB glasses has higher reflectance than the prescription glasses, the prescription glasses enables reading smaller on-screen texts because of its smaller curvature leading to larger reflection pixel size. Note that the conclusion is device-specific and cannot be applied to general BLB-prescription glass comparison. Humans are found more capable in recognizing the reflected texts than SOTA OCR models.

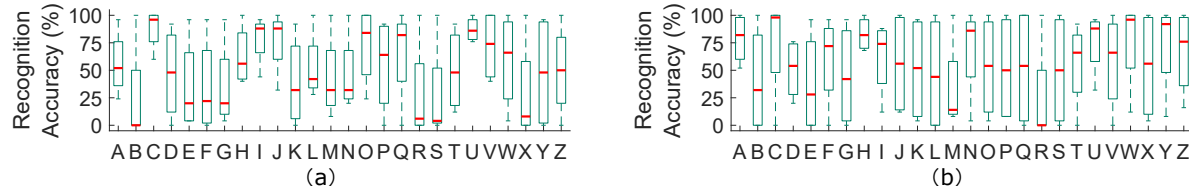


Fig. 8. The human recognition accuracy of different letters with (a) the BLB glasses and (b) the prescription glasses. Letters such as “R” have been found the most difficult to read in the reflections while letters such as “C” and “U” have high recognizability. The difference is mostly due to the simplicity and symmetry in the letters’ structures which lead to smaller degradation of recognizability when the reflections are subject to distortions.

The screen brightness was 100%, and the environmental light intensity was about 100 lux. We then displayed single capital letters (26 letters) on the victim screen with different heights ranging from 20 mm to 7 mm. The victim and adversary laptops had a Zoom [21] session with a video resolution of 1280×720. For each display of the letters, we recorded a 3s video of the victim’s images on the adversary laptop. We then used 8 consecutive frames starting from 1s for MFSR reconstruction and generated one corresponding image for each video. We generated 208 images in total for the 2 glasses each with 4 different sizes.

recognizability Evaluation. In order to evaluate the recognizability of the reconstructed single-letter images and avoid potential bias introduced by the authors’ prior knowledge of the reflections, we acquired recognition accuracy by (1) using multiple SOTA pre-trained deep-learning OCR models including Google Tesseract and Keras CRNN, and (2) conducting a survey² (Appendix J) on Amazon Mechanical Turk (AMT) [10]. For the AMT study, we collected answers from 25 crowdsourcing workers for each reconstructed image, and thus collected 5200 answers in total. We showed to the workers all reconstructed images in a randomized manner without providing them with any information on the original letters on the screen. We asked the workers to provide 3 best guesses of the single letter in each reconstructed image. They were allowed to input the same answer for multiple guesses if they feel confident in a guess, or if they have no clue for making subsequent guesses. The recognizability of the texts in the reconstructed images is then represented by the recognition accuracy, i.e., correctly recognized number of letters over the total number of letters in each case.

B. Recognizability vs. Size

Figure 7 shows the recognition accuracy with the BLB and prescription glasses respectively with different letter sizes. The

AMT accuracy for each letter size is calculated by including all 25 answers for all the 26 letters, i.e., with a denominator of $25 \times 26 = 650$. We picked 4 representative letter sizes for each pair of glasses respectively, and show the top 1, 2, and 3 recognition accuracy. Besides the accuracy, we also use error bars to show the standard deviations. The SOTA OCR models performed considerably worse than AMT workers due to the unique distortions in reflected images (Section III-D) that are unlikely to be included in their training dataset, with the CRNN model giving the highest recognition accuracy as shown in Figure 7.

As shown in the two figures, the prescription glasses generally yield better results for the webcam peeking attack, showing that 10 mm texts can be recognized in the reconstructed images. Although not as good as the prescription glasses, the recognition accuracy with the BLB glasses is also high enough to support efficient peeking attacks against texts of 10-20 mm. Despite the better reflective characteristics of the BLB glasses, the prescription glasses still generate better results due to its smaller curvature, highlighting the risks of the peeking attack even without highly reflective glasses. In addition, in all the cases, there exist noticeable increase in recognition accuracy when the number of guesses increase. For instance, with the prescription glasses, recognizing a 8 mm high letter only has a success rate of around 40%, while it increases to 70% when the adversaries can make 3 guesses.

C. Recognizability vs. Letter

Intuitively, different letters in the alphabet would be recognized with different levels of hardships due to their structural characteristics. Figure 8 shows the box plot of AMT letter-wise recognition accuracy of the four sizes. As shown in the figures, considerable differences in the recognition accuracy exist among different letters. For instance, the letter “R” and “B” have been found the hardest to recognize in both cases of the two pairs of glasses. On the other hand, letters such as “C”, “U”, “I”, and “O” have generally the highest recognizability in

²Institutional Review Board (IRB) No.HUM00208544

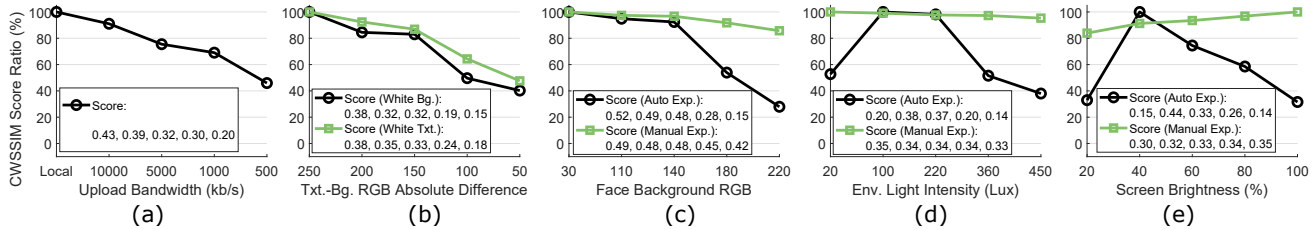


Fig. 9. Effects of impact factors evaluated by CWSSIM scores. The original score numbers are displayed along with the legend at the bottom, and we plot the ratio between each score and the highest score in each case as a percentage. Visualizations of the effects can be found in the appendix.

all the sizes, which we suspect is due to their simple or highly symmetric structures that prevent the recognizability of such letters from dropping too seriously when the texts are down-sampled and occluded. Furthermore, we found letters having similar structures are confused with each other more easily in the recognition. For instance, “J” and “I” are mostly recognized as “I” when the letter size gets small because the distortions to the bottom part of “J” and “L” makes them just like “I” in the reflection images.

D. Network Influence

Since we conducted the experiments with network speed larger than 100 Mbps, the previously shown results almost represent the best-case scenario over a Zoom session. It is also worth discussing how the network capacity may influence the recognizability of the reflections. In addition, video conferencing platforms like Zoom will inevitably introduce noise into the images through video encoding and decoding even with a large enough network bandwidth. To that end, we compared the quality of the reconstructed images under different network bandwidths to that when the video is recorded by the victim’s local device without going through Zoom. A visual demonstration of the effect is shown in Figure 12 which is quantified with CWSSIM scores and shown in Figure 9 (a). We found that when the upload bandwidth is larger than 10 Mbps, the quality of the reconstructed images generally remain the same, and is close to the locally-captured and reconstructed images with a minor degree of added distortions. An upload bandwidth smaller than 10 Mbps starts to undermine the reconstructed image quality over Zoom. When the bandwidth is smaller than 1000 kpbs, the letters get hard to recognize. It’s almost unrecognizable with a bandwidth smaller than 500 kpbs. We also observed that when the bandwidth was larger than 1500 kpbs, Zoom was generally able to maintain a 720p video resolution with a frame rate close to 30 fps (Appendix B).

E. Physical Factors

The recognizability of the reflections is a highly complex multi-variate function over many physical factors. We categorize the factors into 2 groups, namely those mainly affecting the reflection pixel size and those affecting the light SNR. Factors in the first group such as glass-screen distance can already be quantitatively characterized by the reflection model in Section III-B, yet a comprehensive quantitative modeling of light SNR is very challenging due to the requirements of (1) accurately controlling and measuring the physical factors

continuously (2) exhausting all combinations of factors, and (3) developing an accurate optical model for the imaging sensors. Nevertheless, in this work we offer qualitative analysis and quantify representative cases by calculating changes in CWSSIM scores (Figure 9).

In light SNR, the signal portion comes from the light emanated from the screen, reflected by the glasses, and then captured by the imaging sensors corresponding to the area of the screen. Other light captured by sensors in this area can be treated as noise, including environmental light directly hitting the sensors, environmental light reflected by the glasses and screen light reflected by the face background and then hitting the sensors, etc. Counter-intuitively, higher light SNR does not always lead to higher reflection recognizability as we will discuss next. Figure 9 (b-e) show the factors that can change light SNR most significantly besides the image distortions discussed in Section III-D and the glass reflectance which cannot be measured without specialized equipment. (c-e) also inspect how auto exposure and manual (fixed) exposure can affect the light SNR-recognizability relationships in surprisingly different ways by using the laptop built-in webcam and the configurable Nikon Z7 respectively. Besides the anomalies, it also shows that higher-quality imaging sensors are generally more robust to the changes in physical factors.

Text Color Contrast. Intuitively, different colors of texts can affect the reflection recognizability because the texts and screen (not face) background colors produces a certain contrast. Theoretically, both the luma and the chroma components of colors can affect the contrast. But since we find the chroma components have smaller effects which are also tightly coupled with the specific glasses’ reflectance spectrum and thus hard to generalize, we only show the effects of the luma components affecting the webcam in Figure 9 (b) (visualization in Figure 12 (b)) by using the absolute difference in RGB values of gray-scale text and background colors to represent the contrast. As expected, lower contrast (smaller RGB difference) undermines the reflection recognizability. We also find that the combination of dark text and light background colors produces slightly better recognizability than vice versa.

Face Background Reflectance. Face background reflectance is decided by sub-factors such as skin color. We tested different background reflectance by pasting the inner side of the glasses with papers of different gray-scale colors that have the same values for RGB. When the background has a higher reflectance (larger RGB values), more light from

the environment as well as the screen will be reflected by it, increasing the noise portion of the light SNR and thus undermining recognizability of the reflections as shown in Figure 9 (c) (visualization in Figure 12 (c)).

Environment Light Intensity. Theoretically, decrease in the environmental light intensity causes a smaller degree of noise and thus increase the light SNR. This increase of light SNR, however, does not necessarily lead to better recognizability of the reflections in case of webcams which often have auto-exposure control to adjust the overall brightness of the videos they take. When the overall environment is too dark, the webcam’s firmware automatically increase the exposure time trying to compensate for the dark environment. This increase in the exposure time, however, can cause an over-exposure for the reflected contents on the glasses which could have much higher light intensity than the environment, leading to smaller contrast and thus harder-to-read images. Such over-exposure is found in multiple participants’ videos in the user study (Section V-B). On the other hand, the recognizability monotonically increases in the case of manual-exposure cameras such as the Nikon Z7 in manual mode. Figure 9 (d) (visualization in Figure 12 (d)) shows the different behaviors of auto and manual exposure.

Screen Brightness. Screen brightness is the opposite to environmental light intensity in terms of its impact on the reflection recognizability. When the screen is brighter, the signal portion in the light SNR increases and can lead to more readable reflections for manual-exposure cameras. However, auto-exposure of most webcams can again negatively affect the recognizability. Specifically, if the screen gets too bright compared to the environmental lighting condition, the webcams will often adjust their exposure time and ISO based on the dominant environmental light condition, and thus cause over-exposure to the screen reflections. Figure 9 (e) (visualization in Figure 12 (e)) shows the effects.

Summary. The results show that variations in physical conditions can change the actual limits of the attack dramatically. The fact that reflection recognizability does not change monotonically with some factors like environmental light intensity and screen brightness further challenges the attack by making it more difficult to predict the possible outcomes in uncontrolled settings, which will be evaluated in the following sections. .

V. CYBERSPACE TARGET SUSCEPTIBILITY

The evaluations so far are based on the text physical size and carried out in controlled environments to better characterize the user-independent component of the reflection model as well as the range of theoretical limits for webcam peeking. In this section, we start with mapping the limits to common cyberspace objects in order to understand the potential susceptible targets. We then conduct a user study with 20 participants to investigate the feasibility and challenges of peeking these targets in various uncontrolled environments.

TABLE III
TEXT SIZES OF WEB CONTENTS AND SUSCEPTIBILITY TO PRESENT-DAY AND FUTURE WEBCAMS

Target	pt	Cap Height (mm)	Theoretical	User
\mathcal{G}_1 P	12	2.1		
\mathcal{G}_1 H3	14	2.5	☉	
\mathcal{G}_1 H2	18	3.2	☉	☉
\mathcal{G}_1 H1	24	4.3	☉	☉
\mathcal{G}_2 P	21	3.7	☉	☉
\mathcal{G}_2 H3	25	4.3	☉	☉
\mathcal{G}_2 H2	32	5.6	☉	☉
\mathcal{G}_2 H1 (S1)	42	7.4	●	●
\mathcal{G}_3 0% (S2)	56	10	●	●
\mathcal{G}_3 20% (S3)	80	14	●	●
\mathcal{G}_3 40% (S4)	102	18	●	●
\mathcal{G}_3 60%	136	24	●	●
\mathcal{G}_3 80% (S5)	253	35	●	●
\mathcal{G}_3 95% (S6)	340	60	●	●

☉, ☉, and ● mean the text size can be peeked with 4K, 1080p, and 720p cameras respectively. The theoretical column contain predictions of the targets’ susceptibility based on the reflection model and evaluation results in lab settings. The user column contain those based on the user study.

A. Mapping Theoretical Limits to Targets

The plethora of the possible cyberspace textual targets makes it highly difficult to inspect all targets in this study. We thus use web texts as an enlightening example considering their wide use and the relatively mature conventions of HTML and CSS. For example, despite the fact that the default CSS font sizes are decided by web browser vendors separately, we find many of them follow the W3C recommendation [15], where H1, H2, H3 headers’ font sizes are 2, 1.5, 1.17 em respectively. To briefly explain, a text size of x em means the size is x times the current body font size of the web page [20] which is usually the same as the font size of paragraph (P) elements. Nevertheless, we note that web design standards are lacking and designers have a large degree of freedom of choosing their own text designs. Sometimes bigger fonts are preferred in order to make the websites more stylish and eye-catching. In this section, we thus investigate both conventional and more stylish web text sizes. The discussion is based upon (1) a previous report [53] scraping the most popular 1000 websites on Alex web ranking [9], and (2) a manual inspection of 117 big-font websites archived on SiteInspire [11]. We further divide the inspected web texts into the following 3 groups in order to discuss separately how the webcam peeking attack with current and future cameras could have effects on them as summarized in Table III. As pointed out in Section III-B, the conversion between digital point size and physical cap height is dependent on specific user settings such as browser zoom ratio. The cap height values in Table III are thus measured with the Acer laptop with default OS and browser settings as a case study.

\mathcal{G}_1 and \mathcal{G}_2 : The first group represents the median HTML P, H1, H2, H3 texts of the 1000 websites. [53] reports that the median size of the P elements is about 12 pt and H1, H2, H3 sizes are close to the 2, 1.5, 1.17 em ratios recommended [15]. We thus use these point sizes for \mathcal{G}_1 and specify the corresponding cap heights in Table III. The second group represents the largest HTML P, H1, H2, H3 texts of the 1000

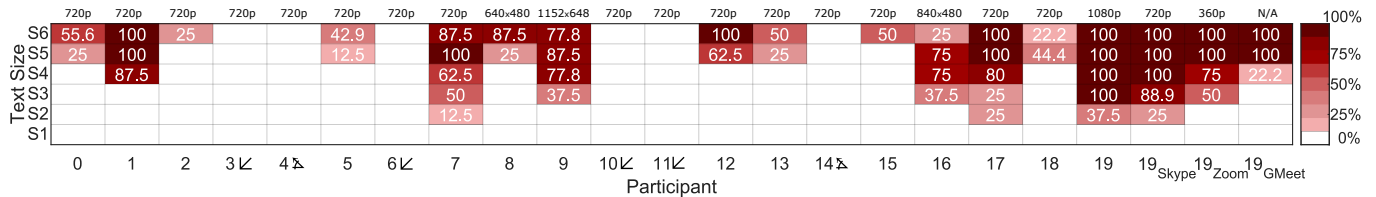


Fig. 10. The recognition results of the reflections collected from user study participants. Participants with \sphericalangle and \sphericaltriangle signs have bad light SNR and viewing angle respectively, which led to no successful recognition.

websites in [53] with the same recommended em ratios for the headers. [53] finds that about 4% of the 1000 websites uses a P size as large as 21 pt. This results in H1, H2, H3 sizes of 25, 32, and 45 pt respectively.

\mathcal{G}_3 : The third group represents the 117 big-font websites’ texts. We manually inspected all the 427 websites archived on SiteInspire [11]. The reason for manual analysis rather than scraping is that many large-font texts on the websites are embedded in the form of images instead of HTML text elements in order to create more flexible font styles. We then selected 117 of them based on the following criteria: (1) The webpage is still active. (2) The largest static texts that enable an adversary to identify the website through google search has a cap height of at least 10 mm when displayed on the Acer laptop. We show the different quantiles of the largest physical cap heights on the 117 websites and the converted point sizes in Table III. We find that most websites in \mathcal{G}_3 are related to art, design, and cinema industry which like to present their stylish design skills but unfortunately make the web peeping attack easier. About 1/3 of the websites are designers’ or studios’ websites that computer science/security researchers may overlook. Furthermore, 72 out of the 117 websites are ranked on Alexa from 38 to 8,851,402 with 5 websites among the top 10,000. .

Based on the results in Figure 7, we hypothesize that the smallest cap heights adversaries can peek using mainstream 720p cameras is 7-10 mm. We then calculate the corresponding limits with 1080p and 4K cameras with Equation 3 and show them in the Theoretical column of Table III. Considering participants are most likely to use 720p cameras, we then choose point sizes S1-S6 in Table III for evaluations in the user study.

B. User Study

The user study³ (Appendix J) is designed in the following challenge-response way: An author generates HTML files each with one randomly selected headline sentence containing 7-9 words⁴ from the widely-used “A Million News Headlines” dataset [51]. Only each word’s first letter is capitalized. The participants display the HTML page in their browsers when they are recorded, and another author acting as the adversary tries to recognize the words from the videos containing the 20 participants’ reflections without knowing the HTML contents

³Institutional Review Board (IRB) No.ZDSYHS-2022-5

⁴Uniform lengths (e.g., all 8 words) are avoided to prevent the adversary from guessing the words by knowing how long the sentences are.

by using the same techniques as in Section IV. We then calculate the percentage of correctly recognized words.

Data Collection. Each participant was given 6 HTML files of increasing point sizes from S1 to S6 as shown in Table III. Note that the 6 sizes are specified in point size in HTML so that user-dependent factors such as screen size and browser zoom ratio can be studied (Equation 1). The participants display each HTML files on their own computer display in their accustomed rooms and behave normally as in video conferences. We allow participants to choose their preferred environmental lighting condition except asking them to avoid other close light sources besides the screen in front of their face. The reason is that we found a close frontal light source can seriously decrease light SNR, which can potentially be used as a physical mitigation against this attack but prevents us from examining the impact of all the other factors. We did not tell the participants to stay stationary and let them behave normally as in browsing screen contents. Their webcam, either built-in or external, record their image for 30 seconds for each HTML file. To test the impact of video conferencing platforms while ensuring realistic workload at the same time, we record the 20 participants’ videos locally first, and then record participant 19’s videos again (with different HTML contents) from the adversary side through Skype, Zoom, and Google Meet meetings. Another reason that we didn’t perform video-call recording for the majority of the participants is that we believe network bandwidth and video call quality as artifacts will be constantly improved in a rapid way [4] compared to other user-dependent physical factors that we focus on in this study.

We asked the participants to report their user-dependent parameters including screen resolution (N_{os}), screen physical size (H_{sr}), OS and browser zoom ratio (s_{os}, s_b) webcam resolution in Equation 1, webcam resolution (N) in Equation 3, and the type of their glasses. Some other physical factors including environmental light intensity, screen brightness, and glass-screen distance, and the physical size of displayed texts are difficult to be measured by the participants themselves and are not reported. We thus estimated the values of these factors by utilizing their videos (see Appendix H). Lastly, the reflectance and curvature of the glasses are not included in this study since their measurement requires specialized facilities.

General adversary Recognition Results. The recognition accuracy achieved by the adversary is shown in Figure 10. The percentage of participants subjected to the attack against S6-S1 are 70%, 60%, 30%, 25%, 15%, and 0% respectively. .

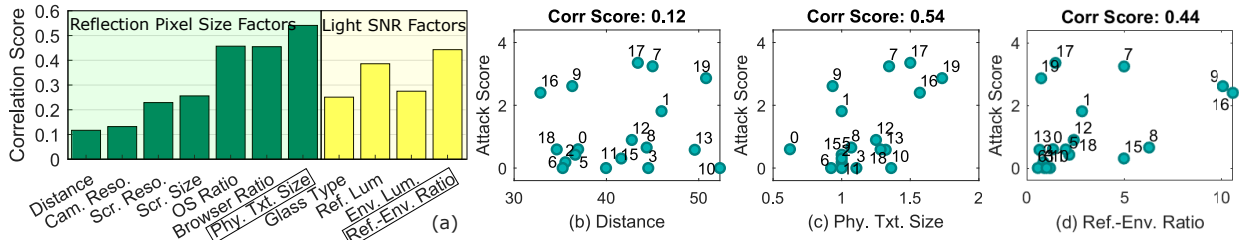


Fig. 11. (a) The degree of influence of different factors on the reflection recognition performance evaluated by the correlation scores. Factors highlighted with boxes are computed with other raw factors according to our model. (b-d) The joint distribution of three factors and the recognition results.

Videos of participant 7 and 17 using 720p cameras allowed the adversary to achieve 12.5% and 25% accuracies on recognizing S2. Videos of participant 16 using a 480p camera allowed the adversary to achieve an 37.5% accuracy on recognizing S3. These results translate to the predicted susceptible targets with cameras of different resolutions as listed in the User column of Table III, where 720p webcams pose threats to large-font webs (\mathcal{G}_3) and future 4K cameras pose threats to various header texts on popular websites (\mathcal{G}_1 and \mathcal{G}_2). As expected, this result is slighted worse than the theoretical limits in the table. Besides the more diverse and challenging environments, we believe other reasons include: (1) Texts in the user study are mostly lower-case and have smaller physical size than the upper-case letters in Section IV. (2) Recognizing words can be more difficult than recognizing single letters. (3) Glass curvatures as small as the one of the prescription glasses used in Section IV are relatively rare. Besides the attack limits, the results also verifies the attack’s robustness to viewing angles as predicted in Section III-B since only 2 participants (4 and 14) did not generate usable reflections due to the problem of out-of-range vertical angles. 3 participants (3, 10, and 11) yield 0% accuracy due to a very low light SNR, while another 3 participants (7, 16, and 18) suffered from the problem of over-exposure which led to worse accuracy than they could have generated under ideal lighting.

For the video call recordings of participant 19, we observed only slight degradation in the recognition accuracy for Skype, which maintained a 720p video resolution in the data collection process. Zoom suffered from larger degradation because it was only able to support a 360p connection at the time of collection. We suspect it was because the video call between the two authors was transoceanic and led to a maximum Zoom bandwidth below 1200 kbps observed, which matches with the results in Section IV-D. The web-based Google Meet platform only enabled peeking S4 as compared to the S2 of Skype. We could not identify its video resolution but observed generally worse video quality than even 360p Zoom.

Underlying Reasons. Given the recognition results and the reported/calculated parameters, it will be interesting to find out the dominant reasons enabling easier webcam peeking by analyzing the correlation between the recognition results and different factors. To that end, we turn each participant’s results (6 sizes) into a single value. We hereby define an empirical *Attack Score* that is a rectified weighted sum of the recognition

accuracy of the six text sizes tested:

$$A_p = \sum_{i=1}^6 w^{i-1} \times \tanh(2a_{p,i})$$

where $a_{p,i}$ is the accuracy (in $[0, 1]$) for participant p text size i and w is a small-text emphasis factor.

Figure 11 (a) shows correlation scores with 11 factors that affect reflection pixel size (left) and light SNR (right) respectively when $w = 1.5$. The glass type includes prescription (15/20) and prescription with BLB coatings (5/20). The physical text size and reflection-environment light ratio highlighted in the boxes are two compound factors. In short, the physical text size represents the ratio between the actual physical size of texts displayed on each participant’s screen and the case study values in Table III and is calculated with Equation 1 with other raw factors such as browser zoom ratios. The reflection-environment light ratio represents how strong the screen brightness is compared to the environmental light intensity and is calculated by dividing glass luminance by environmental luminance (see Appendix H). Basically, these two compound factors represent our model’s prediction to reflection pixel size and light SNR and is found to generate higher correlation scores than the other raw factors, which validates the effectiveness of our models. Figure 11 (b-d) further show the joint distribution of the attack score and three representative factors. It can be seen from (b) that the 40 mm screen-glass distance used in the evaluation of Section IV is about the average of the participants’ values, and distances of these participants actually only have very weak correlation with the easiness of webcam peeking attack. Figure 11 (d) suggests that when the screen brightness-environmental light intensity ratio gets lower than a certain threshold, the likelihood of preventing adversaries from peeking is very high, which can be considered as a temporary mitigation.

VI. DISCUSSION

A. Proposed Near-Term Mitigations

Given the threats, it is worthwhile exploring feasible mitigations that can be applied immediately. We notice that platforms such as Zoom provide virtual filters, including non-transparent cartoon glasses that can completely block the eye areas and thus eliminate the reflections. Other software-based approaches that support better usability involve fine-tuned blurring of the glass area. Although the platforms do not

support it now, we have implemented a real-time eyeglass blurring prototype that can inject a modified video stream into the video conferencing software (See Appendix I). More sophisticated software mitigations could leverage eyeglass reflection removal algorithms [61] from the CV research community. We tested multiple such algorithms, yet none achieve high-fidelity reflection removal on the real-time data and all require processing time of at least several seconds for each frame. We think offloading the processing of such algorithms to clouds may improve its performance. A more timely and accessible approach involves users modifying the dominant physical factors identified in this work to reduce the reflection pixel or light SNR. For example, they might simply place a lamp facing their face whose light increase the noise portion of light SNR.

B. Long-Term Defenses

We believe that a sensor system should strive to provide only what data is necessary to complete a function in security-sensitive scenarios. Prescient research from 20 years ago predicted privacy consequences of pervasive cameras [30], [62]. Camera technology continues to improve both in the spacial and time domain, enabling the exposure of finer grain visual information. Cameras are getting more capable than what average users can understand—unwittingly exposing information beyond what users intend to share. Privacy-sensitive users take draconian measures such as disabling webcams entirely. We believe there are design philosophies that strike a more nuanced long-term tradeoff between privacy and utility of webcam technology.

The fundamental privacy design challenge with webcam technology is “oversensing”. The oversensing observation [29] finds that overly-capable sensors can provide too much information to downstream processing—more data than is needed to complete a function, such as a meaningful face-to-face conversation. This oversensing leads to a violation of the sensor equivalent to the classic *Principle of Least Privilege (PoLP)* [59]. We believe long-term protection of users ought to follow a PoLP (perhaps a Principle of Least Pixels) as webcam hardware and computer vision algorithms continue to improve.

Previous research [29] proposed to filter raw sensor data streams to regulate the amount of accessible information and to create access control mechanisms for allowing different categories of users to acquire different levels of information. We believe this approach could work well for webcam data, but will require privacy enhancing technology catering to video streaming within the software stack. Currently, platforms such as Zoom attempt to enhance privacy by providing background blurring functionality, but there are three major problems. First, such privacy-enhancing functionality is turned off by default, which essentially means the users themselves need to understand the subtle risks of high performance cameras. Second, such blur is a binary on/off gadget and does not allow users to adjust the level of protection based on their evaluation of how sensitive the current session is. Third, such

protection is relatively niche and cannot be applied to defend other emerging threats such as webcam peeking.

Thus, we recommend that future infrastructure and privacy-enhancing modules follow the PoLP not just for software, but for the camera data streams themselves. In sensitive conversations, the infrastructure could provide only the minimal amount of information needed and allow users to incrementally grant higher access privileges to the other parties. For example, PoLP blurring techniques might blur all objects in the video meeting at the beginning and then intelligently unblur what is absolutely necessary to hold natural conversations.

VII. RELATED WORK

The problem of screen reconstruction is a long-studied challenging problem. In this section, we analyze the past works that served as the foundations for our thinking in the context of video conferencing today and in the predicted future.

Screen Peeking Using Cameras. Screen-peeking with cameras through optical emanation reflections have been explored in previous works. In 2008, Backes et al. [27] showed that adversaries can use off-the-shelf telescopes and DSLR cameras to spy victims’ LCD monitor screen contents from up to 30m away by utilizing the reflective objects that can be commonly found next to the monitor screen such as teapots placed on a desk. In 2009, the authors [26] took the attack to the next level by addressing the challenges of motion blur and out-of-focus blur by performing deconvolution on the photos with Point Spread Functions (PSF). Our work differs from these previous works by exploiting the victims’ own webcams in video conference for a remote attack. Such changes call for different imaging enhancing techniques due to the different types of image distortions. In addition, reflective objects on the desks and human eyes cannot be easily utilized (see Appendix A for more detailed explanation). We thus exploit the glasses people wear to video conferences as a modern attack vector. [66] proposed a relevant idea of using adversary-controlled webcam to detect changes in webpage links’ colors for inferring visited websites. It requires the adversary to take control over the victim’s webcam with malicious web modules and exploits coarse-grain color variations, while our work studies more natural attack vectors in video conferencing and investigate the limits of textual reconstruction.

Screen Content Reconstruction With Other Emanations. Besides the direct optical emanations from the screen that we exploit in this work, previous works also explored other channels such as electromagnetic radiation [49], [50], [64] and acoustic emanations [41]. Reconstructing screen contents with such emanations usually requires using additional eavesdropping hardware that is placed close to the victims by the adversary. On the other hand, our work exploits the victim’s own webcams, making the attack more accessible and low-cost.

Remote Eavesdropping Via Audio/video Calls. Similar to our work, such attacks assume the adversary and victim are both participants of an audio/video conference, and the

adversary can eavesdrop privacy-sensitive information by analyzing the audio/video channels. For example, Voice-over-IP attacks for keystroke inference eavesdrop the victim’s keyboard inputs by utilizing timing and/or spectrum information embedded in the keystroke acoustic emanations [32], [34], [38], [63]. Recently, Sabra et al. [58] proposed works solving the problem of inferring keystrokes by analyzing the dynamic body movements embedded in the videos during a video call. Hilgefert et al. [46] spies victims’ nearby objects through virtual backgrounds in video calls by carrying out foreground-background analysis and accumulating background pixels. In contrast, our work explores the related problem of the limits of screen textual contents reconstruction using only the optical reflections from participants’ glasses that are embedded in the videos.

VIII. CONCLUSION

In this work, we characterized the threat model of the webcam peeking attack in video conferencing settings. We developed mathematical models that describe the relationship between the attack limits and different user-dependent factors. The analysis enables the prediction of future threats as webcam technology evolves. We conducted experiments both in controlled lab settings and with a user study. Results showed that present-day 720p cameras pose threats to the contents on users’ screens when users browse certain big-font websites. Future 4K cameras are predicted to allow adversaries to reconstruct various header texts on popular websites. Our proposed mitigations leverage the Principle of Least Privilege and more judiciously blurs foreground images by default to reduce unwitting leakage of textual reflections.

ACKNOWLEDGEMENT

This work is supported by the Archimedes Center for Health and Device Security. Any opinions, findings, and conclusions or recommendations expressed in this material are those of the authors and do not necessarily reflect the views of the funding institute.

REFERENCES

- [1] Converting diagonal field of view and aspect ratio to horizontal and vertical field of view. <http://vrguy.blogspot.com/2013/04/convert-diagonal-field-of-view-and.html>, 2013.
- [2] Webcam Field of View . <https://www.telehealth.org.nz/assets/Uploads/1511-webcam-field-of-view.pdf>, 2015.
- [3] Approximate Focal Length for Webcams and Cell Phone Cameras. <https://learnopencv.com/approximate-focal-length-for-webcams-and-cell-phone-cameras/>, 2016.
- [4] Cisco Annual Internet Report (2018–2023) White Paper. <https://www.cisco.com/c/en/us/solutions/collateral/executive-perspectives/annual-internet-report/white-paper-c11-741490.html>, 2020.
- [5] Could 2021 Be The Year Remote Working Becomes The New Normal? <https://www.forbes.com/sites/enriquequedans/2021/12/30/could-2021-be-the-year-remote-working-becomes-the-newnormal/>, 2020.
- [6] Schott AG: Transmittance of optical glass. https://www.schott.com/d/advanced_optics/5b1f5065-0587-4b3f-8fc7-e508b5348012/, 2020.
- [7] The most maddening part about working from home: video conferences. . <https://www.washingtonpost.com/technology/2020/03/16/remote-work-video-conference-coronavirus/>, 2020.
- [8] Acer Predator 15. <https://www.acer.com/ac/en/IN/content/predator-model/NH.Q1YSI.001>, 2021.

- [9] Alexa SEO and Competitive Analysis Software. <https://www.alexa.com/>, 2021.
- [10] Amazon Mechanical Turk. <https://www.mturk.com/>, 2021.
- [11] Big Type Websites. <https://www.siteinspire.com/websites?categories=22>, 2021.
- [12] Blue Light Blocking Glasses Market Size 2021 with a CAGR of 7.7% , Research by Business Opportunities, Top Companies data report covers, globally Market Key Facts and Forecast to 2025. <https://www.wboc.com/story/43536337/blue-light>, 2021.
- [13] Blue Light Blocking Glasses on Amazon. <https://www.amazon.com/gp/product/B07VBFSY33/>, 2021.
- [14] Cheese. <https://wiki.gnome.org/Apps/Cheese>, 2021.
- [15] Default style sheet for HTML 4. <https://www.w3.org/TR/CSS2/sample.html>, 2021.
- [16] For better or worse, working from home is here to stay. <https://www.cnn.com/2021/03/11/one-year-into-covid-working-from-home-is-here-to-stay.html>, 2021.
- [17] Nikon Z7. <https://www.nikonusa.com/en/nikon-products/product/mirrorless-cameras/z-7.html>, 2021.
- [18] Samsung Notebook 9. <https://www.samsung.com/hk/pc/notebook-9-np900x5m-k03/>, 2021.
- [19] Shot Noise. https://en.wikipedia.org/wiki/Shot_noise, 2021.
- [20] Web Style Sheets CSS tips & tricks: EM. <https://www.w3.org/Style/Examples/007/units.en.html#units>, 2021.
- [21] Zoom. <https://zoom.us/>, 2021.
- [22] Zoom System requirements for Windows, macOS, and Linux. <https://support.zoom.us/hc/en-us/articles/201362023>, 2021.
- [23] Aries Ardit. Adjustable typography: an approach to enhancing low vision text accessibility. *Ergonomics*, 47(5):469–482, 2004.
- [24] Aries Ardit and Jianna Cho. Serifs and font legibility. *Vision research*, 45(23):2926–2933, 2005.
- [25] Melanie Arntz, Sarra Ben Yahmed, and Francesco Berlingieri. Working from home and covid-19: The chances and risks for gender gaps. *Intereconomics*, 55(6):381–386, 2020.
- [26] Michael Backes, Tongbo Chen, Markus Dürmuth, Hendrik PA Lensch, and Martin Welk. Tempest in a teapot: Compromising reflections revisited. In *2009 30th IEEE Symposium on Security and Privacy*, pages 315–327. IEEE, 2009.
- [27] Michael Backes, Markus Dürmuth, and Dominique Unruh. Compromising reflections-or-how to read lcd monitors around the corner. In *2008 IEEE Symposium on Security and Privacy (sp 2008)*, pages 158–169. IEEE, 2008.
- [28] Alexander Bick, Adam Blandin, and Karel Mertens. Work from home after the covid-19 outbreak. *CEPR Discussion Paper*. 2020.
- [29] Connor Bolton, Kevin Fu, Josiah Hester, and Jun Han. How to curtail oversensing in the home. *Communications of the ACM*, 63(6):20–24, 2020.
- [30] Michael Boyle, Christopher Edwards, and Saul Greenberg. The effects of filtered video on awareness and privacy. In *Proceedings of the 2000 ACM conference on Computer supported cooperative work*, pages 1–10, 2000.
- [31] Anthony S Carlson. A comparison of blue-light transmissions through blue-control lenses. *African Vision and Eye Health*, 78(1):1–7, 2019.
- [32] Stefano Ceconello, Alberto Compagno, Mauro Conti, Daniele Lain, and Gene Tsudik. Skype & type: Keyboard eavesdropping in voice-over-ip. *ACM Transactions on Privacy and Security (TOPS)*, 22(4):1–34, 2019.
- [33] Jung Won Cha. The study about measuring method in radius of eyeglasses lens curvature by using keratometer. *Journal of Korean Ophthalmic Optics Society*, 17(2):127–133, 2012.
- [34] Alberto Compagno, Mauro Conti, Daniele Lain, and Gene Tsudik. Don’t skype & type! acoustic eavesdropping in voice-over-ip. In *Proceedings of the 2017 ACM on Asia Conference on Computer and Communications Security*, pages 703–715, 2017.
- [35] Zechuan Deng, René Morissette, and Derek Messacar. Running the economy remotely: Potential for working from home during and after covid-19. *Statistics Canada*. 2020.
- [36] Keyan Ding, Kede Ma, Shiqi Wang, and Eero P Simoncelli. Image quality assessment: Unifying structure and texture similarity. *arXiv preprint arXiv:2004.07728*, 2020.
- [37] Rodger J Elble. Tremor. In *Neuro-geriatrics*, pages 311–326. Springer, 2017.
- [38] Fürkan Elilob, Uğur Sarac, and İşin Erer. Realistic eavesdropping attacks on computer displays with low-cost and mobile receiver system. In

- 2012 Proceedings of the 20th European Signal Processing Conference (EUSIPCO), pages 1767–1771. IEEE, 2012.
- [39] Leslie G Farkas, Marko J Katic, and Christopher R Forrest. International anthropometric study of facial morphology in various ethnic groups/races. *Journal of Craniofacial Surgery*, 16(4):615–646, 2005.
- [40] Sina Farsiu, M Dirk Robinson, Michael Elad, and Peyman Milanfar. Fast and robust multiframe super resolution. *IEEE transactions on image processing*, 13(10):1327–1344, 2004.
- [41] Daniel Genkin, Mihir Pattani, Roei Schuster, and Eran Tromer. Synesthesia: Detecting screen content via remote acoustic side channels. In *2019 IEEE Symposium on Security and Privacy (SP)*, pages 853–869. IEEE, 2019.
- [42] William T Ham, Harold A Mueller, and David H Sliney. Retinal sensitivity to damage from short wavelength light. *Nature*, 260(5547):153–155, 1976.
- [43] WT Ham, JJ Ruffolo, HA Mueller, AM Clarke, and ME Moon. Histologic analysis of photochemical lesions produced in rhesus retina by short-wave-length light. *Investigative ophthalmology & visual science*, 17(10):1029–1035, 1978.
- [44] William T Ham Jr, John J Ruffolo Jr, Harold A Mueller, and DuPont Guerry III. The nature of retinal radiation damage: dependence on wavelength, power level and exposure time. *Vision research*, 20(12):1105–1111, 1980.
- [45] Atsuki Higashiyama, Yoshikazu Yokoyama, and Koichi Shimono. Perceived distance of targets in convex mirrors. *Japanese Psychological Research*, 43(1):13–24, 2001.
- [46] Jan Malte Hilgert, Daniel Arp, and Konrad Rieck. Spying through virtual backgrounds of video calls. In *Proceedings of the 14th ACM Workshop on Artificial Intelligence and Security*, pages 135–144, 2021.
- [47] Brien A Holden, Timothy R Fricke, David A Wilson, Monica Jong, Kovin S Naidoo, Padmaja Sankaridurg, Tien Y Wong, Thomas J Naduvilath, and Serge Resnikoff. Global prevalence of myopia and high myopia and temporal trends from 2000 through 2050. *Ophthalmology*, 123(5):1036–1042, 2016.
- [48] Mohammad Moinul Islam, Vijayan K Asari, Mohammed Nazrul Islam, and Mohammad A Karim. Video super-resolution by adaptive kernel regression. In *International Symposium on Visual Computing*, pages 799–806. Springer, 2009.
- [49] Markus G Kuhn. Electromagnetic eavesdropping risks of flat-panel displays. In *International Workshop on Privacy Enhancing Technologies*, pages 88–107. Springer, 2004.
- [50] Markus G Kuhn. Security limits for compromising emanations. In *International Workshop on Cryptographic Hardware and Embedded Systems*, pages 265–279. Springer, 2005.
- [51] Rohit Kulkarni. A Million News Headlines, 2018.
- [52] Tsz Wing Leung, Roger Wing-hong Li, and Chea-su Kee. Blue-light filtering spectacle lenses: optical and clinical performances. *PloS one*, 12(1):e0169114, 2017.
- [53] Michael Li. I studied the fonts of the top 1000 websites. Here’s what I learned. <https://dribbble.com/stories/2021/04/26/web-design-data-fonts>, 2021.
- [54] Tony Lindeberg. Scale invariant feature transform. 2012.
- [55] Ko Nishino and Shree K Nayar. Corneal imaging system: Environment from eyes. *International Journal of Computer Vision*, 70(1):23–40, 2006.
- [56] Tuba Ozdemir, Adnan Saglam, Firdevs Banu Ozdemir, and Ali Ünsal Keskiner. The evaluation of spectral transmittance of optical eye-lenses. *Optik*, 127(4):2062–2068, 2016.
- [57] Tatsiana Palavets and Mark Rosenfield. Blue-blocking filters and digital eyestrain. *Optometry and Vision Science*, 96(1):48–54, 2019.
- [58] Mohd Sabra, Anindya Maiti, and Murtuza Jadhwal. Zoom on the keystrokes: Exploiting video calls for keystroke inference attacks. *arXiv preprint arXiv:2010.12078*, 2020.
- [59] Jerome H Saltzer and Michael D Schroeder. The protection of information in computer systems. *Proceedings of the IEEE*, 63(9):1278–1308, 1975.
- [60] Mehul P Sampat, Zhou Wang, Shalini Gupta, Alan Conrad Bovik, and Mia K Markey. Complex wavelet structural similarity: A new image similarity index. *IEEE transactions on image processing*, 18(11):2385–2401, 2009.
- [61] Tushar Sandhan and Jin Young Choi. Anti-glare: Tightly constrained optimization for eyeglass reflection removal. In *Proceedings of the IEEE Conference on Computer Vision and Pattern Recognition*, pages 1241–1250, 2017.
- [62] Andrew Senior, Sharath Pankanti, Arun Hampapur, Lisa Brown, Ying-Li Tian, Ahmet Ekin, Jonathan Connell, Chiao Fe Shu, and Max Lu. Enabling video privacy through computer vision. *IEEE Security & Privacy*, 3(3):50–57, 2005.
- [63] Iliia Shumailov, Laurent Simon, Jeff Yan, and Ross Anderson. Hearing your touch: A new acoustic side channel on smartphones. *arXiv preprint arXiv:1903.11137*, 2019.
- [64] Wim Van Eck. Electromagnetic radiation from video display units: An eavesdropping risk? *Computers & Security*, 4(4):269–286, 1985.
- [65] Zhou Wang, Alan C Bovik, Hamid R Sheikh, and Eero P Simoncelli. Image quality assessment: from error visibility to structural similarity. *IEEE transactions on image processing*, 13(4):600–612, 2004.
- [66] Zachary Weinberg, Eric Y Chen, Pavithra Ramesh Jayaraman, and Collin Jackson. I still know what you visited last summer: Leaking browsing history via user interaction and side channel attacks. In *2011 IEEE Symposium on Security and Privacy*, pages 147–161. IEEE, 2011.
- [67] Jianchao Yang and Thomas Huang. Image super-resolution: Historical overview and future challenges. In *Super-resolution imaging*, pages 1–34. CRC Press, 2017.
- [68] B Zelzer, A Speck, A Langenbacher, and T Eppig. Theoretical model for design and analysis of protection eyewear. *Zeitschrift für Medizinische Physik*, 23(2):120–128, 2013.
- [69] Lin Zhang, Lei Zhang, Xuanqin Mou, and David Zhang. Fsim: A feature similarity index for image quality assessment. *IEEE transactions on image processing*, 20(8):2378–2386, 2011.

APPENDIX A REFLECTIVE OBJECT ANALYSIS

Comparing the webcam setting with the previous works’ DSLR-telescope setting [26], [27], we had a few key observations: (1) It’s very challenging to utilize reflections in human eyes. Due to the very large curvature of human eyes ($f_g \approx 4$ mm [55]), the reflections of the normal texts on the screens are of extremely small pixel size, which is further aggravated by the low pixel resolution of the webcams. According to the reflection calculations in Section III-B, most on-screen texts will be smaller than 1 pixel in the webcam captures. In addition, the amount of light reflected from eyes are inherently small and thus requires a long exposure time for acquisition [26], which is not supported by the webcams as pointed out above. (2) It’s also infeasible to utilize reflective objects such as teapots on a desk next to the screens. Not like in [26], [27] where the attacker can arbitrarily tune the aiming angles of their DSLR-telescope systems, the webcams of the victims are at fixed positions and angles, and out of the attacker’s control. Aiming the webcam to a nearby object reflecting the screen’s contents is thus infeasible. Even worse, most webcams are facing upwards because of the screen angle as shown in Figure 1. This almost eliminates all reflective objects close to the screen that are placed on desks as the possible peeking targets. The only exception is the glasses the victim wears, which have moderate reflective property and curvature so that the screen contents can be potentially reflected without being shrunk to invisible. Given the above observations, we thus decide to focus on reading reflections on the victims glasses in this work.

APPENDIX B EXPERIMENT EQUIPMENT

The Acer laptop [8] has a screen width of 38 cm and height of 190 cm and a 720p built-in webcam. The OS is Ubuntu 20.04. The OS and browser zoom ratios are default (100%).

All the photos and videos are collected with the Cheese [14] webcam application. The photos are in PNG format and the videos are in WEBM format. The Samsung laptop used as the attacker device has OS Windows 10 Pro. The recordings are collected with OBS Studio in MP4 format.

The pair of BLB glasses [13] has lenses with a horizontal and vertical chord length of 5 cm and 4 cm respectively, and a focal length (f_g) of 8 cm. The pair of prescription glasses [13] has lenses with a horizontal and vertical chord length of 6 cm and 5 cm respectively, and a focal length of 50 cm.

Nikon Z7: The photos are in JPEG format (highest quality) and the videos are in MP4 format. We compared these formats with the compression-less (raw) photo and video formats provided by Nikon Z7 while didn't find obvious difference in the image quality.

APPENDIX C WEBCAM PARAMETER ESTIMATION

The manufacturer of the laptop built-in webcams often do not share information about the webcam focal length f and imaging sensor physical size W . In this case, further estimation needs to be made. The term $\frac{f}{W}$ is a function of the vertical field-of-view (FoV) of the webcams. Specifically, the FoV angle α can be written as

$$\alpha = 2 \tan^{-1} \frac{W}{2f}$$

Considering that typical webcams have a diagonal FoV of in the range $70 - 90^\circ$, we can convert it to a typical vertical FoV of about $40 - 50^\circ$ for a 720p webcam and thus get $\frac{f}{W}$ approximately in the range of $1.1 - 1.4$ [1]–[3]. Although this value will vary from webcam to webcam, it should be able to offer us good insights into the approximate range of reflection pixel size.

APPENDIX D VIEWING ANGLE MODEL DERIVATION

In order to find a mapping from the rotation angle θ to the light-emission point P_3 on the screen, the key is to find the slope of line P'_2P_3 which intersects with the screen. Since $P'_1P'_2$ bisects $P'_2P'_4$ and $P'_2P'_3$, we denote the slope of these three lines as b_1, b_2, b_3 respectively, and have

$$b_3 = \frac{b_2 - 2b_1 - b_1^2 b_2}{b_1^2 - 2b_1 b_2 - 1}$$

To calculate b_1 and b_2 , the coordinate of P'_1 and P'_2, P_4 can be denoted as,

$$\begin{cases} P'_1 : ((s - 2f_g)\cos\theta, (s - 2f_g)\sin\theta) \triangleq (C, D) \\ P'_2 : (x_0\cos\theta - y_0\sin\theta, x_0\sin\theta + y_0\cos\theta) \triangleq (A, B) \\ P'_2 : (s + d, 0) \triangleq (E, 0) \end{cases}$$

and thus

$$b_1 = \frac{B - D}{A - C}, \quad b_2 = \frac{B}{A - E}$$

The last missing piece is the coordinate of P_2 , which is denoted as $P_2 : (x_0, y_0) = (r \times \cos\alpha, r \times \sin\alpha)$, where

$$\begin{cases} r = \sqrt{(\frac{C}{2})^2 + (\sqrt{R^2 - (\frac{C}{2})^2} - (R - s))^2} \\ \alpha = -\arcsin(\frac{C}{2r}) \end{cases}$$

APPENDIX E ZOOM UNDER LOW BANDWIDTH

Although bandwidths smaller than 10 Mbps led to worse image quality in our observations, Zoom generally remained stable when the bandwidth was larger than 4M bps. When it got smaller than 4 Mbps, however, we found Zoom will first experience a short period of aggravated packet loss, and then rapidly decrease the video resolution to compensate for it. Nevertheless, the video resolution, which is a crucial factor for the webcam peeking attack, will not remain low forever. Soon it will be increased again by sacrificing the frame rate as well as the compression loss. Zoom will still try to recover high frame rate later by further increasing the video compression loss. Through our experiments, we noticed that when the bandwidth was larger than 1500 kbps, Zoom was able to maintain a 1280*720 resolution with a frame rate very close to 30 fps. In comparison, Zoom suggests an upload bandwidth of at least 1.2 Mbps for 720p 30 fps videos in a 1:1 video call and 2.6 Mbps in a group call [22]. Reduced bandwidth leads to both decreased frame rate and increased video compression loss, causing the worsening of the reconstructed images' quality in our tests.

APPENDIX F VISUALIZATION OF FACTORS' IMPACT

Figure 12 shows the original reflections of Figure 9.

APPENDIX G OBJECT METRICS FOR REFLECTION QUALITY

Besides the manual or machine-learning based reflection recognition accuracy that we discuss in Section IV, it is also important to find easily computed objective metrics that enable people to preliminarily determine the quality of reflected texts in a rapid and scalable way. To this end, we embody this notion of reflection quality in the similarity between the reflected texts and the original templates. We compared multiple widely-used image structural and textural similarity indexes including structural similarity Index (SSIM) [65], complex-wavelet SSIM (CWSSIM) [60], feature similarity (FSIM) [69], deep image structure and texture similarity (DISTS) [36] as well as self-built indexes based on scale invariant feature transform (SIFT) features [54]. We found CWSSIM, which is robust to various rigid transforms, produces the best match with human perception results. We thus use the CWSSIM similarity score between reflections and templates as the reflection quality metric, which spans the interval $[0, 1]$ with larger numbers meaning more similar and thus higher quality. It is worth noting that the reflections having high CWSSIM scores is only a necessary yet not sufficient condition for them to

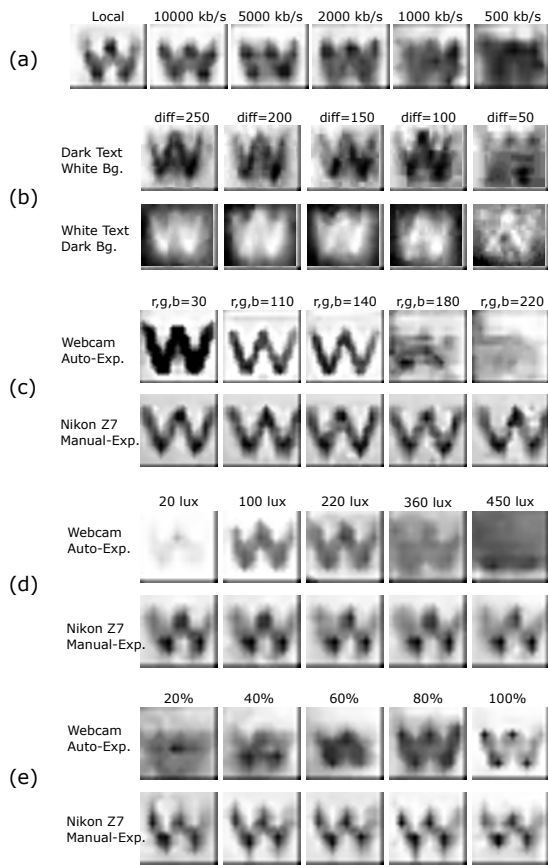


Fig. 12. (a) The comparison between reconstructed images when the video is recorded locally on the victim device and over Zoom with different network upload bandwidths. (b) Changes of reflection recognizability with different text-background color contrast. (c) Changes of reflection recognizability with different background colors (reflectance). We tested gray-scale colors with the same RGB values, which have relatively uniform reflectance on the visible light spectrum. (d) Changes of reflection recognizability under different environmental light intensity. (e) Changes of reflection recognizability with different screen brightness.

be recognizable. Through our experiments, we find that in order to be recognizable by either human or machine learning algorithms, the CWSSIM score usually needs to be larger than 0.28.

APPENDIX H USER STUDY FACTOR ESTIMATION

The overall environmental light intensity and is estimated by taking the average pixel luminance in the video frames. The screen brightness is estimated by taking the average pixel luminance in glass area containing the screen reflections. The glass-screen distance is estimated by the physical average physiognomical face height [39] and physiognomical pixel height in the video frames using similar formula as Equation 2.

APPENDIX I GLASS BLURRING DEFENSE PROTOTYPE

Figure 13 demonstrates the application of a real-time defense algorithm from our prototype developed with Dlib, OpenCV, and pyvirtualcam Python packages. It uses Dlib’s

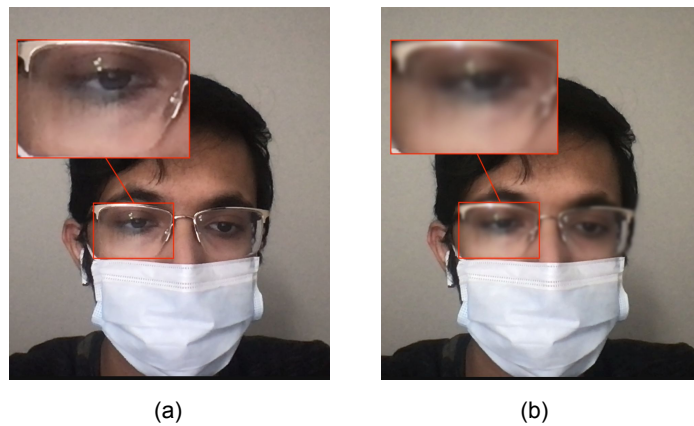


Fig. 13. The comparison between the user’s eyeglass reflections during a Zoom meeting (a) from the original webcam input, and (b) from the defense algorithm’s virtual camera.

frontal face detector to initially detect the user’s face before predicting the location of 68 facial landmarks. Then, the program uses OpenCV to narrow the region of interest from the user’s entire face to just the eyeglasses region. OpenCV extracts this new region and applies a blur to mitigate the attacker’s ability to interpret any reflections. Pyvirtualcam allows us to feed this new video stream into Open Broadcasting Software’s (OBS) virtual camera, essentially treating our program as another ordinary webcam. After running the program, the user can select the virtual camera as their video input instead of the original webcam to directly feed the defense algorithm into their video conference platform. The program only has an approximately 0.035 second delay per frame, so there is no noticeable drop in framerate. Future development should move away from blurring and towards stronger reflection removal algorithms while maintaining an efficient runtime.

APPENDIX J HUMAN SUBJECTS RESEARCH INFORMATION

AMT. The AMT study received IRB waiver from the authors’ institutes. The survey results downloaded from AMT website are de-anonymized by only keeping their answers and deleting all other information including worker IDs. The results on the AMT website are deleted. We provided compensations of \$18/h for the workers.

User Study. The participants were anonymized with random orders. No personal information other than the videos and questionnaires was collected. The HTML files they used were created randomly by the authors and do not involve the participants’ private information or contain any unethical or disrespectful information. The participants’ videos were used only for this research and not disclosed to third parties or used for other purposes.